Int. J. Microgravity Sci. Appl., 36 (2) (2019)
360204 DOI: 10.15011//jasma.36.360204

IIII Original Paper IIII

Effect of Heat Loss on Hydrothermal wave Instability in Half-Zone Liquid Bridges of High Prandtl NumberFluid

Sorachi FUJIMOTO [1], Toru OGASAWARA [2], Asumi OTA [1], Kosuke MOTEGI [2] and Ichiro UENO [1, 3]

Abstract

We investigate the effect of heat transfer through a free surface on the primary instability of thermocapillary-driven convection in a geometry of so-called half-zone liquid bridge of high Prandtl number fluid. The target liquid bridge is a straight whose aspect ratio $\Gamma = H/R$ is mainly kept at 2.0, where H and R are the height and the radius of the bridge, respectively. We focus on the flow fields induced by the instability; it is found that the bifurcation diagram exhibits a significant difference between the cases of the Prandtl number Pr = 16 and 28. The effect of gravity level is also examined in order to discuss qualitatively the induced flow fields after the transition obtained in the ground-based experiments as well as in on-orbit experiments so-called 'Dynamic Surf' in the Japan Experiment Module 'Kibo' aboard the International Space Station.

Keyword(s): Hydrothermal wave instability, Dynamic Surf, Half-zone liquid bridge, High Prandtl number fluid, Heat transfer
Received 22 January 2019; Accepted 18 April 2019; Published 30 April 2019

1. Introduction

Flow instability induced by the thermocapillary effect in a high Prandtl number fluid, or, so-called hydrothermal wave (HTW) instability, has been an attractive topic since Smith & Davis [1)] and Xu & Davis [2)] towards applications such as material processings, crystal growths and cleaning processes. Especially with a geometry of half-zone liquid bridge, in which an amount of liquid is 'bridged' between the coaxial cylindrical rods, a number of research have been conducted in order to understand the transition process of the induced convection. Kamotani et al. [3)] triggered a range of discussion on sensitivity of the instability to the heat transfer through the free surface. In the induced convection with this geometry with high Prandtl number (Pr) fluid, it has been known that the flow field exhibits a transition from two-dimensional time-independent 'steady' state to three-dimensional time-dependent 'oscillatory' one [4–9)]. Such transition is known as the primary one due to HTW instability. Recently Ogasawara et al. [10)] illustrated the existence of secondary instability even for high Pr fluids. The thermal-flow fields in traveling regime after the primary instability and before the secondary instability have a single fundamental frequency, and they seem rigid in the reference frame rotating with HTW [e.g., 11,12)]. Kamotani et al. [3)] indicated that the onset condition for the primary instability is drastically affected by changing the ambient-gas temperature. Effect of the ambient-gas flow around the liquid bridge was then illustrated by experimental [13–16)] and numerical [13,15,17–20)] approaches. Series of microgravity experiments in the Japanese Experiment Module 'Kibo' aboard the International Space Station (ISS) were conducted [21,22)] as a part of the Japan-US joint project known as 'Dynamic Surf,' and would be conducted [23)] as a part of the Japan-Europe joint project known as 'JEREMI (Japanese-European Research Experiments on Microgravity Instability)' focusing on this problem. According to the knowledge accumulated through the previous researches, it has been found that the heat loss through the free surface destabilizes the flow fields [7,17,19,22)], whereas the heat gain stabilizes those [3,14,22)]. In a wider range of heat transfer, on the other hand, it was also indicated that the heat-loss condition would bring stabilizing effect on the induced convection [17,19)]. It was also indicated that the standing-wave-type oscillatory mode emerges more stably in the induced oscillatory convection after the onset of primary instability in the microgravity experiments with high Pr fluids [9)].

One has to accumulate knowledges on physical mechanism to select the flow patterns induced by the thermocapillary-effect under the effect of heat transfer through the free surface for more precise prediction of the transition condition as well as the flow patterns. Xun et al. [24)] conducted a linear stability analysis for the liquid bridge of Pr = 16 and the aspect ratio $\Gamma = H/R = 1.8$ (H and R are the height and radius of the liquid bridge, respectively) in order to illustrate the effects of heat loss to the primary instability, and indicated the flow patterns as well as the transition conditions as a function of heat transfer ratio. In order to lead comprehensive understandings of the transition mechanism in the liquid bridge of higher Pr employed in the ground- [e.g., 4,7,25)] and on-orbit experiments such as 'MEIS (Marangoni Experiments in

1 Div. Mechanical Engineering, School of Science & Technology, Tokyo University of Science, 2641 Yamazaki, Noda, Chiba 278-8510, Japan.
2 Dept. Mechanical Engineering, Faculty of Science & Technology, Tokyo University of Science, 2641 Yamazaki, Noda, Chiba 278-8510, Japan.
3 Research Institute for Science & Technology, Tokyo University of Science, 2641 Yamazaki, Noda, Chiba 278-8510, Japan.
(E-mail: ich@rs.tus.ac.jp)

Space [e.g., 8,9,26–28])' as well as 'Dynamic Surf,' it is indispensable to conduct theoretical analyses dealing with the effect of heat transfer through the free surface on the transition problems.

In the present study, we examine the effect of heat transfer through the free surface on the hydrothermal wave instability in a tall liquid bridge of Pr = 28 by linear stability analysis. Note that the Prandtl number concerned is still too small comparing to those employed in the on-orbit experiments (Pr $\gtrsim$ 70); this research work is conducted to illustrate that a slight change of Pr brings significant effects on the transition for the first place. Note as well that this value of Pr corresponds to the one of the test fluid, which has been widely used in the ground experiments.

2. Methods

2.1 Formulation of problem

The target geometry is a straight cylindrical liquid bridge sustained between the coaxial circular disks (**Fig. 1**). The radius of the disks is R, and the height of the liquid bridge (or, the dis-tance between the disks) is H. The shape of the liquid bridge in the present study is fixed; aspect ratio $\Gamma = 2.0$, and volume ratio $V/V_0 = 1.0$, where V is the volume of the liquid and V_0 is the volume of the cylinder between the rods as $\pi R^2 H$. We consider a situation that a mean surface tension of the liquid is large enough to neglect any static and dynamic deformations of the liquid bridge. The temperatures of the top disk at $z^* = H$ and the bottom one at $z^* = 0$ are kept constant at $T^* = T^*_{\mathrm{H}}$ and $T^* = T^*_{\mathrm{C}}$, respectively. The temperature difference between the disks is described $\Delta T^* = T^*_{\mathrm{H}} - T^*_{\mathrm{C}} > 0$. The surface tension $\gamma(T^*)$ is assumed to depend on the temperature T^* linearly, that is, $\gamma(T^*) = \gamma\left(T^*_{\mathrm{C}}\right) + \gamma_T\left(T^* - T^*_{\mathrm{C}}\right)$, where γ_T indicates the temperature coefficient of the surface tension $\gamma_T = \partial\gamma/\partial T^*$. In the present study it is assumed that $\gamma_T = \text{const.} < 0$.

Heat transfer between the liquid bridge and the ambient gas is considered by introducing a constant heat transfer coefficient h in order to describe the heat flux on the free surface. The temperature in the ambient gas is assumed to be constant at the bottom rod temperature, that is, $T^*_\infty = T^*_{\mathrm{C}}$ as introduced by the previous studies [24,29]. Heat transfer through the free surface of the liquid bridge is controlled via non-dimensional Biot number defined as $\mathrm{Bi} = -(\mathrm{hH})/\lambda$, where λ is the thermal conductivity of the liquid.

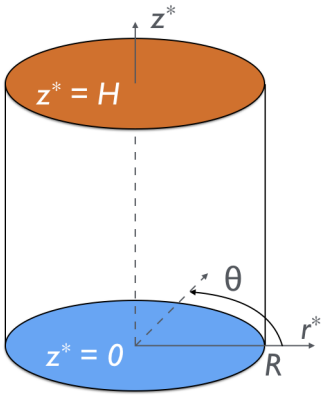

Fig. 1 Target geometry: half-zone liquid bridge of aspect ratio $\Gamma = H/R = 2.0$.

We consider a Newtonian and incompressible fluid in the liquid bridge. The governing equations are (1) Navier-Stokes, (2) continuity, and (3) thermal energy equations. These equations are non-dimensionalized by considering the scales H, $U_0 = (|\gamma_T|\Delta T^*)/(\rho\nu)$, ρU_0^2, and H/U_0 for the length, velocity, pressure, and time, respectively. ρ and ν are the density and the kinematic viscosity of the liquid, respectively. Non-dimensional velocity vector $\mathbf{u}$ consists of u_r, u_θ and u_z in r-, θ- and z-direction components, and non-dimensional temperature T is defined as $\left(T^* - T^*_{\mathrm{C}}\right)/\Delta T^*$. The properties except the surface tension are independent of the temperature. The governing equations are described as follows;

$$\frac{\partial \mathbf{u}}{\partial t} + (\mathbf{u}\cdot\nabla)\mathbf{u} = -\nabla P + \mathrm{Re}^{-1}\nabla^2\mathbf{u} + \frac{\mathrm{Bd}}{\mathrm{Re}}\mathbf{Te_z}, \tag{1}$$

$$\nabla\cdot\mathbf{u} = 0, \tag{2}$$

$$\frac{\partial T}{\partial t} + (\mathbf{u}\cdot\nabla)T = \frac{1}{\mathrm{RePr}}\nabla^2 T, \tag{3}$$

where Re indicates the thermocapillary Reynolds number defined as $\mathrm{Re} = |\gamma_{\mathrm{T}}|\Delta\mathrm{T}^*\mathrm{H}/(\rho\nu^2)$, and Bd indicates the dynamic Bond number defined as $\rho g\beta\mathrm{H}^2/|\gamma_{\mathrm{T}}|$. The gravity is described by g, and the thermal expansion coefficient by β. Note that the dynamic Bond number is also defined as Gr/Re where Gr expresses the Grashof number.

We apply no-slip boundary condition on both of the end disks, and so-called 'thermocapillary boundary condition' over the free surface, which demands the thermocapillary shear stresses on the free surface are balanced by bulk shear stresses [1,29]. The boundary conditions in non-dimensional manner are described as follows; $\mathbf{u}(\mathbf{z}=\mathbf{1},\,\mathbf{0}) = \mathbf{0}$, $T(z=1) = 1$, and $T(z=0) = 0$ on the both end disks. On the free surface (at $r = 1/\Gamma$), $\mathbf{u}\cdot\mathbf{e_r} = \mathbf{0}$, $\mathbf{S}\cdot\mathbf{e_r} + (\mathbf{I_3} - \mathbf{e_r}\mathbf{e_r})\cdot\nabla\mathbf{T} = \mathbf{0}$, $\nabla T\cdot\mathbf{e_r} + \mathrm{Bi}(\mathrm{T} - \mathrm{T}_\infty) = 0$, where $\mathbf{S} = \nabla\mathbf{u} + (\nabla\mathbf{u})^{\mathrm{T}}$ is the stress tensor, $\mathbf{e_r}$ the unit vector in a radial direction, $\mathbf{I_3}$ the identity matrix, and T_∞ the ambient temperature.

2.2 Numerical methods and validation

Linear stability analysis in this study is based on Motegi et al. [30] The flow and thermal fields $\Phi = (u_r, u_\theta, u_z, P, T)^{\mathrm{T}}$ are decomposed into the basic field $\overline{\Phi} = (\overline{u_r}, \overline{u_\theta}, \overline{u_z}, \overline{P}, \overline{T})^{\mathrm{T}}$ and the disturbances $\hat{\phi} = (\hat{u_r}, \hat{u_\theta}, \hat{u_z}, \hat{P}, \hat{T})^{\mathrm{T}}$ as $\Phi(r,\theta,z,t) = \overline{\Phi}(r,\theta,z) + \hat{\phi}(r,\theta,z,t)$ by assuming that the disturbances are (I) small enough as $\|\hat{\phi}\| \ll 1$, and (II) are expanded to the normal modes as $\hat{\phi}(r,\theta,z,t) = \tilde{\phi}(r,z)\exp(\mathrm{i}m\theta + \xi t) + \mathrm{c.c.}$, where $\mathrm{i}^2 = -1$, m is the azimuthal wave number, ξ is the complex growth rate, and *c.c.* the complex conjugate. In the present study, we target the thermal-flow field of $m = 0$, 1 and 2 in the analysis, and never consider the higher m because of the high Γ of the liquid bridge [5,7]. The basic flow is axisymmetric and steady, so that $\partial_t\overline{\Phi} = \partial_\theta\overline{\Phi} = \overline{u_\theta} = 0$. Govern-

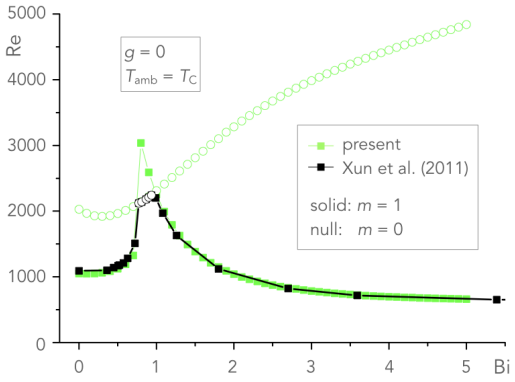

Fig. 2 Neutral curves for liquid bridge of (Pr, Γ) = (16, 1.8) under zero gravity ($0g_0$) condition. Prediction by Xun et al.[24] is also illustrated.

ing equations (1-3) for the basic flow are described by the stream function–vorticity formulation. The Stokes stream function Ψ and vorticity ζ are introduced as $\overline{u_r} = (1/r)\partial_z\Psi$, $\overline{u_z} = -(1/r)\partial_r\Psi$, $\zeta = \partial_z\overline{u_r} - \partial_r\overline{u_z}$, and we substitute them into the governing equations. We adopt boundary conditions as follows: $\Psi = \partial_z\Psi = 0$ on the both end disks, $\overline{T} = 0$ for $z = 0$ and $\overline{T} = 1$ for $z = 1$, $\overline{\Phi} = \zeta - \partial_z\overline{T} = 0$ on the free surface (at $r = 1/\Gamma$), and $\overline{\Phi} = \zeta = \partial_r\overline{T} = 0$ on the central axis of the liquid bridge (at $r = 0$).

We put Φ into the governing equations (1-3), then the disturbance is governed by partial differential equation as follows;

$$\left[\partial_t\mathcal{S} + \mathcal{L} + \mathrm{d}\mathcal{N}\left(\overline{\Phi}\right)\right]\hat{\phi} = \mathcal{N}\left[\hat{\phi},\hat{\phi}\right], \tag{4}$$

where the operators $\mathcal{S}$, $\mathcal{L}$ and $\mathcal{N}[\Phi,\Phi]$ are described as follows (*see the next page*);

(*followed by Eqs. 5–8 on the next page*) As we assume (I) the disturbance is small as aforementioned, the disturbance is governed by a partial differential equation:

$$\left[\partial_t\mathcal{S} + \mathcal{L} + \mathrm{d}\mathcal{N}\left(\overline{\Phi}\right)\right]\hat{\phi} = 0. \tag{9}$$

Equation 9 is discretized using the central difference scheme. Then $\tilde{\phi}$ and ξ are determined by solving the generalized eigenvalue problems obtained. When the basic flow is neutrally stable (*i.e.*, $\Re(\xi) = 0$), the Reynolds number is denoted as the critical Reynolds number $\mathrm{Re_c}$. Employing the Arnoldi method[31] we calculated about 30 eigenvalues with large real parts to prevent overlooking any neutral curves.

Two-dimensional basic thermal-flow fields $\overline{\Phi} = (\overline{u_r}, \overline{u_\theta}, \overline{u_z}, \overline{P}, \overline{T})^{\mathrm{T}}$ are solved with a mesh of $(N_r, N_z) = (67, 120)$ and $(133, 120)$. Since we convince ourselves that the coarse mesh is fine enough to resolve the basic thermal-flow fields $\overline{\Phi}$, we employ the mesh of $(N_r, N_z) = (67, 120)$ in the followings. The governing equations for the disturbances are solved with a mesh of $(N_r, N_\theta, N_z) = (67, 61, 120)$ through this work. The effect of the grid numbers are examined with a finer mesh system of $(N_r, N_\theta, N_z) = (133, 61, 240)$.

We first conduct the linear stability analysis for the liquid bridge of (Pr, Γ, Bd) = (16, 1.8, 0), which are the same as Xun et al.[24] to validate our code. **Figure 2** illustrates the on-set conditions of the oscillatory convections under the condition of $T^*_\infty = T^*_{\mathrm{C}}$ for the ambient gas temperature. Note that the value of Bi by Xun et al.[24] is converted under the present definition; the Biot number in Xun et al.[24] was defined with the radius of the liquid bridge as the characteristic length, whereas that in the present study is defined with the height of the liquid bridge. It is found that the eigenfunction with $m = 2$ does not emerge as the most dangerous thermal-flow field under this condition as Xun et al.[24] predicted. We convince ourselves the present code reproduces almost perfectly the predictions of the onset condition with the most dangerous flow patterns in terms of the eigenfunctions. The difference in the predicted threshold ranges within a few percent. The grid-size effect will be discussed in §3 with the results of the onset conditions for the primary instabilities.

3. Results and Discussion

3.1 Under zero gravity

Figure 3 illustrates the nuetral curves in terms of Re (or, critical Reynolds number $\mathrm{Re_c}$) against the Biot number Bi for different aspect ratio Γ under zero gravity condition (top), and corresponding surface-temperature deviations $\hat{T}$ over the free surface (bottom): rows (1) and (2) indicate the results under Γ = 1.5 and 2.0, respectively. It is found that the most dangerous azimuthal wave number is $m = 1$ under these conditions. Not only the eigenfunction with $m = 2$ but also that with $m = 0$ become more stable against the perturbations, thus the nuetral curves never appear in the range of this figure. Note that the surfaces of the liquid bridge are drawn by reflecting the corresponding aspect ratio for the sake of visibility; the liquid-bridge height H is considered as the characteristic length, so that the non-dimensional heights for all cases are of unity. In the liquid bridge of Γ = 1.5, flow field with one kind of eigenfunction emerges in a range of Bi concerned. The critical Reynolds number decreases as Bi. This nuetral curve is called as branch (a) hereafter. The flow fields with this eigenfunction accompany with the temperature deviation over the free surface propagating from the hot disk to the cold disk as indicated in the bottom of the figure: A pair of relatively cold and relatively hot spots emerge near the heated disk by monitoring the surface temperature deviation. So that one realizes an oscillatory convection with an azimuthal mode number $m = 1$. The cold spot stretches toward the cooled disk as its width becomes narrower to form a local cold line as getting close to the cooled disk. Such flow pattern of branch (a) was observed in the microgravity experiments[8,21] as well as numerical simulations[16]. The

$$\mathcal{S} = \begin{pmatrix} 1 & 0 & 0 & 0 & 0 \\ 0 & 1 & 0 & 0 & 0 \\ 0 & 0 & 1 & 0 & 0 \\ 0 & 0 & 0 & 0 & 0 \\ 0 & 0 & 0 & 0 & 1 \end{pmatrix}, \tag{5}$$

$$\mathcal{L} = \begin{pmatrix} -\mathrm{Re}^{-1}\left(\Delta - \mathrm{r}^{-2}\right) & 2\mathrm{Re}^{-1}\mathrm{r}^{-2}\partial_\theta & 0 & \partial_r & 0 \\ -2r^{-2}\mathrm{Re}^{-1}\partial_\theta & -\mathrm{Re}^{-1}\left(\Delta - \mathrm{r}^{-2}\right) & 0 & r^{-1}\partial_\theta & 0 \\ 0 & 0 & -\mathrm{Re}^{-1}\Delta & \partial_z & -\mathrm{Bd}/\mathrm{Re} \\ \partial_r + r^{-1} & r^{-1}\partial_\theta & \partial_z & 0 & 0 \\ 0 & 0 & 0 & 0 & -\mathrm{Ma}^{-1}\Delta \end{pmatrix}, \tag{6}$$

$$\mathcal{N}\left[\hat{\phi},\hat{\phi}\right] = \begin{pmatrix} -\left(\hat{u}_r\partial_r\hat{u}_r + r^{-1}\hat{u}_\theta\partial_\theta\hat{u}_r + \hat{u}_z\partial_z\hat{u}_r - r^{-1}\hat{u}_\theta\hat{u}_\theta\right) \\ -\left(\hat{u}_r\partial_r\hat{u}_\theta + r^{-1}\hat{u}_\theta\partial_\theta\hat{u}_\theta + \hat{u}_z\partial_z\hat{u}_\theta - r^{-1}\hat{u}_r\hat{u}_\theta\right) \\ -\left(\hat{u}_r\partial_r\hat{u}_z + r^{-1}\hat{u}_\theta\partial_\theta\hat{u}_z + \hat{u}_z\partial_z\hat{u}_z\right) \\ 0 \\ -\left(\hat{u}_r\partial_r T + r^{-1}\hat{u}_\theta\partial_\theta T + \hat{u}_z\partial_z T\right) \end{pmatrix}, \tag{7}$$

$$\mathrm{d}\mathcal{N}\left(\overline{\Phi}\right)\hat{\phi} = \mathcal{N}\left[\overline{\Phi},\hat{\phi}\right] + \mathcal{N}\left[\hat{\phi},\overline{\Phi}\right] \tag{8}$$

relatively cold region, as well as hot region, rotates azimuthally at the same azimuthal velocity along the z direction but with a phase difference at each z position. Thus the thermal wave seems propagate from the hot disk to the cold disk without changing its spatial distribution all over the free surface.

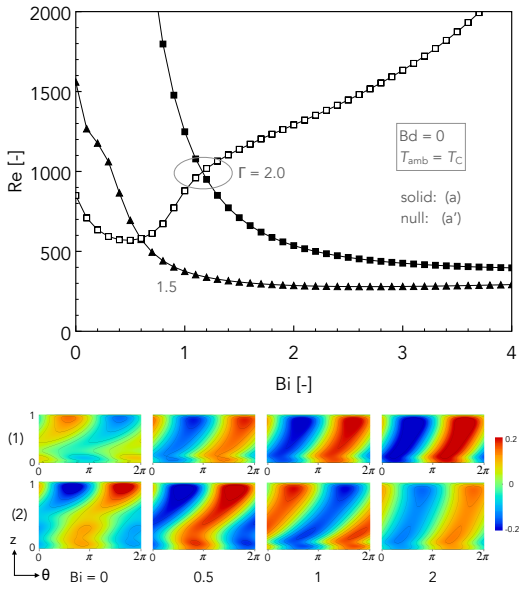

Fig. 3 Nuetral curves against the Biot number Bi (top), and corresponding surface-temperature deviations $\hat{T}$ over the free surface (bottom) for liquid bridge of (Pr, Bd) = (28, 0) under Γ = (1) 1.5 and (2) 2.0. The surfaces of the liquid bridge are drawn by considering the aspect ratio. The most dangerous wave number is found to be $m = 1$ for the whole conditions concerned.

In the case of the liquid bridge of Γ = 2.0, on the other hand, it is found that two different branches with the same $m = 1$ structure appear against Bi. We indicate that the newly emerged branch is the most unstable eigenfunction in a region of Bi $\lesssim 1.2$, and the branch (a) becomes the most unstable one in the higher Bi. The distribution of the surface-temperature deviation for newly arisen branch is similar in quality to that for the branch (a). That is, there exists a pair of relatively hot and cold areas cover the free surface of the liquid bridge, and the thermal wave propagates obliquely from the hot to cold disks. It is found that the basic flow patterns in $r-z$ plane resemble each other as well. We call this new branch as the branch (a').

Here we estimate the grid-size effect for evaluating $\mathrm{Re_c}$. **Table 1** indicates the thresholds under Γ = 2.0 and Bd = 0 as a function of Bi. There exist differences of 2 to 4% for small Bi and about 0.2% for large Bi between the thresholds with coarse and fine grids. In the following we will discuss with the results obtained by employing coarse grid.

Basic thermal-flow fields under (Pr, Γ, Bd) = (28, 2.0, 0) for various Bi are illustrated in **Fig. 4**. These fields are obtained under the conditions as shown in **Fig. 3** (bottom) with the surface temperature deviations over the free surface. Left and right halves of the liquid bridge for each frame indicate the distributions of streamline and temperature T, respectively. Under these conditions, the corresponding eigenfunction of thermal-flow fields for (i)-(iii) is the branch (a'), and that for (iv) is the branch (a). For the flow with the branch (a') the position of the vortex center as seen in the streamline distribution slightly moves downward as Bi. In the adiabatic case (or Bi = 0), one can see two vortices in the flow

Table 1 Grid-size effect for evaluating $\mathrm{Re_c}$ under $\Gamma = 2.0$ and $\mathrm{Bd} = 0$.

	$(N_r, N_\theta, N_z) =$ (67,61,120)	(133,61,240)
Bi = 0	849.6282	884.1281
0.1	709.5720	730.5526
0.2	634.8126	650.0903
0.3	593.1553	605.9405
0.4	572.9500	584.7789
0.5	569.1695	581.2153
0.6	580.8571	594.5563
3.5	406.9298	407.6780
3.6	404.3758	405.1561
3.7	402.1424	402.9518
3.8	400.1979	401.0334
3.9	398.5143	399.3736
4.0	397.0726	398.0722

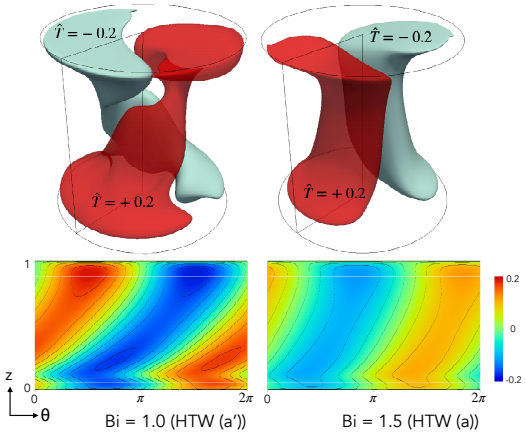

Fig. 5 Bird-eye views of the isosurfaces of the temperature deviation $\hat{T} \pm 0.2$ (top), and corresponding surface-temperature deviations $\hat{T}$ over the free surface (bottom) for Bi = 1.0 with branch (a') (left) and Bi = 1.5 with branch (a) (right) under (Pr, Γ, Bd) = (28, 2.0, 0)

field. As increasing Bi the flow field evolves with a single vortex, and the surface temperature decreases for both branches. In comparing (iii) with the branch (a') and (iv) with the branch (a), one cannot detect apparent variation especially in the flow field with streamline distribution for the basic flow.

Generally in the experimental researches, the flow patterns had been discussed through the spatio-temporal observations of the surface temperature and/or its deviation, for instance, by employing the infrared camera [12,16]. The present results imply that one would not be able to distinguish the induced flow pattern only by the observation of the surface temperature distributions nor by the monitoring the basic thermal-flow field if any knowledges not be accumulated on induced oscillatory flow patterns before conducting the experiments.

We thus focus on the three-dimensional structure of the eigenfunction after the onset of instability. **Figure 5** (top) illustrates the bird-eye views of the isosurfaces of the temperature deviation $\hat{T} \pm 0.2$. This figure illustrates the spatial distribution of the temperature deviation under Bi = 1.0 for the branch (a') (left) and under Bi = 1.5 for the branch (a) (right). The figure also illustrates corresponding distributions of the temperature deviations over the free surface (bottom). In the case of Bi lower than that for the co-dimension two point with the branch (a'), the isosurfaces of the temperature deviation distribute inside the liquid bridge in twisted shape; when one focuses on positive $\hat{T}$, for instance, there exist a pair of large structures near the hot and cold disks, and those large structures are connected with thin and twisted structure of isosurface. The azimuthal positions of those large structures near the hot and cold disks are separated with a difference of azimuthal position about π. If one pays attention to the distribution of the temperature deviation over the free surface, the difference of azimuthal position between the relatively hot region near the hot disk and the relatively cold region near the cold disk is of about π. In the case of Bi higher than that for the co-dimension two point with the branch (a), on the other hand, the isosurfaces of $\hat{T}$ exhibits rather straight shape along z direction. As seen in the case of the branch (a'), there exist a pair of large structures near the hot and cold disks. The connecting part of the isosurface between those large structures are different from the case of the branch (a'); those large structures are connected with thin and almost flat structure of isosurface. Another difference lies in the azimuthal positions of those large structures near the hot and cold disks. In this case, the large structures near the hot and cold disks are located with a much less difference of azimuthal position. Such distribution of the large structures of $\hat{T}$ with less difference in azimuthal direction is also seen in the shape of the surface temperature deviations over the free surface. Thus, the propagation angle or inclination angle of the thermal wave over the free surface become less than that for the branch (a').

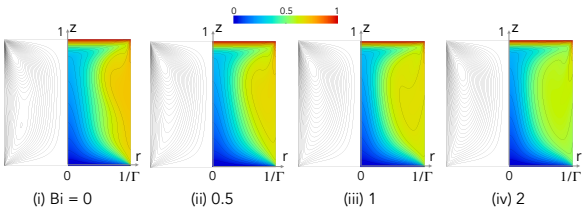

Fig. 4 Basic thermal-flow fields under (Pr, Γ, Bd) = (28, 2.0, 0) for various Bi. These fields are obtained under the conditions as shown in Fig. 3 (bottom) with the surface temperature deviations over the free surface. Left and right halves of the liquid bridge for each frame indicate the distributions of streamline and temperature T, respectively. Corresponding eigenfunction of thermal-flow fields for (i)-(iii) is the branch (a'), and that for (iv) is the branch (a).

3.2 Effect of gravity

We then pay attention to the effect of gravitational acceleration. **Figure 6** illustrates the neutral curves under Bd = 0.34 (plots in red). This condition corresponds to a system of a liquid bridge of 0.75 mm in radius under g = $1g_0$ condition. The most dangerous wave number is also found to be $m = 1$ under this condition. In the figure the results under zero gravity as shown in **Fig. 3** are also indicated (in black). It is found that the critical Reynolds number is not affected by the gravity significantly in a region of Bi $\gtrsim 0.7$; the neutral curves almost coincide with those under zero gravity. That is, the branch (a') becomes the most unstable eigenfunction in small Bi region, and the most unstable eigenfunction is switched to the branch (a) in Bi $\gtrsim 1.2$. In a range Bi $\lesssim 0.7$ for the branch (a'), the flow field with $m = 1$ becomes stabilized, or the critical Reynolds number becomes slightly higher or stabilized, due to the gravitational effect. We find that a new branch with another eigenfunction emerges in the region of almost adiabatic (Bi ~ 0), which becomes the most unstable eigenfunction. This newly-arisen branch is called as (b) hereafter.

Basic thermal-flow fields under (Pr, Γ, Bd) = (28, 2.0, 0.34) for various Bi are illustrated in **Fig. 7**. Left and right halves of the liquid bridge for each frame indicate the distributions of streamline and temperature T, respectively. Corresponding eigenfunction of thermal-flow fields for (i)-(ii) is the branch (b), that for (iii)-(iv) is the branch (a'), and that for (v)-(vi) is the branch (a). There exist two vortices in the flow field (i) with the branch (b); similar basic flow field is also observed under the zero gravity condition (see **Fig. 4 (i)**). Such flow field was clearly observed in the microgravity experiment on ISS with the fluid of higher Pr fluid [21]. As increasing Bi, a pair of vortices disappear in the thermal-flow fields with the branches (a) and (a'). In the case of the branch (b), we have a steeper temperature gradient in r direction in the region of outer-bottom half of the liquid bridge due to the double vortices. Such tendencies are detected in the case of Bd = 0 as well. It is rather difficult to indicate significant effect of the gravity on the basic thermal-flow fields comparing to the effect of Bi.

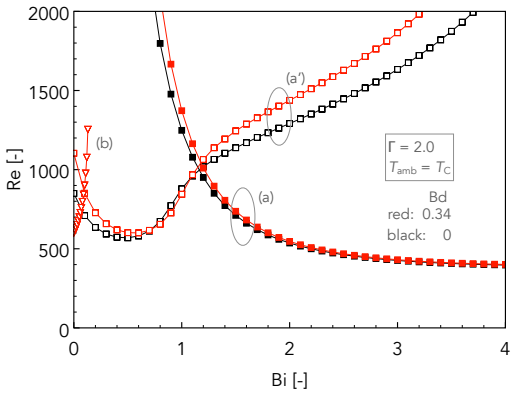

Fig. 6 Nuetral curves against the Biot number Bi for liquid bridge of Pr = 28 with Γ = 2.0 under dynamic Bond number Bd = 0.34 (plots in red). The most dangerous wave number is found to be $m = 1$ for the whole conditions concerned. The results under Bd = 0 for the same liquid bridge (as shown in Fig. 3) is also plotted (in black).

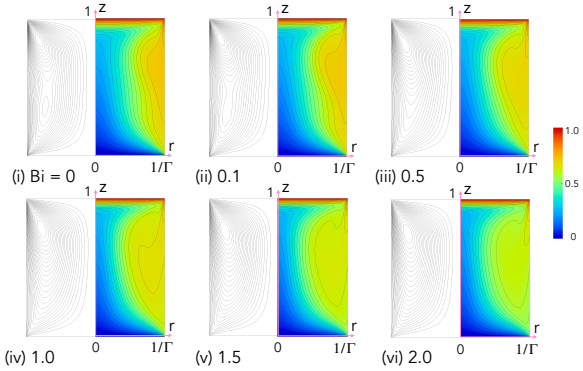

Fig. 7 Basic thermal-flow fields under (Pr, Γ, Bd) = (28, 2.0, 0.34) for various Bi. Left and right halves of the liquid bridge for each frame indicate the distributions of streamline and temperature T, respectively. Corresponding eigenfunction of thermal-flow fields for (i)-(ii) is the branch (b), that for (iii)-(iv) is the branch (a'), and that for (v)-(vi) is the branch (a).

The temperature deviations inside the liquid bridge and over the free surface in this flow pattern are illustrated in **Fig. 7**. The isosurfaces of $\hat{T}$ become rather compact, and shift to a region close to the hot disk. There exists a large structure near the hot disk as seen in the cases of the branches (a) and (a'). The isosurfaces shrink their shape, and the bottom region of the isosurfaces becomes apart from the cold disk. We cannot see any thin regions in the isosurfaces at the middle height as seen in the cases of HTWs (a) and (a'), but the isosurfaces exhibit bulge-like structure there. This must result in a region with a significant variation of the surface temperature at midheight as well as the region near the hot disk, but not near the cold disk (see the bottom frames in the figure). The surface-temperature deviation in the branch (b) also consists of a pair of hot and cold spots as that in the branch (a). In the branch (b), each spot spreads toward the cold disk almost vertically, not obliquely. That is, the relatively hot and cold regions spread straightly toward the cold disk; those regions rotates azimuthally at the same azimuthal velocity along the z direction in matching the phase. High-amplitude $\hat{T}$ emerges not only near the hot disk but also in the middle height. The azimuthal positions of those high-amplitude $\hat{T}$ are almost the same. Near the cold disk, on the contrary, the amplitude of the $\hat{T}$ becomes smaller comparing to the cases of the branches (a) and (a').

Such flow pattern corresponding to the branch (b) was observed in the ground experiments with a small-scale liquid bridge [16], and also in the microgravity experiment known as 'Dynamic Surf' conducted in the Japanese Experiment Module 'Kibo' on the In-

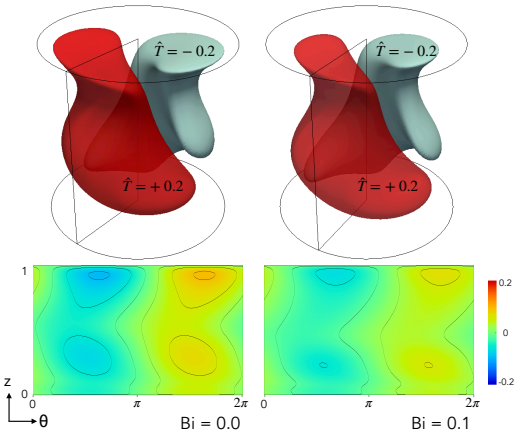

Fig. 8 Bird-eye views of the isosurfaces of the temperature deviation $\hat{T} \pm 0.2$ (top), and corresponding surface-temperature deviations $\hat{T}$ over the free surface (bottom) for Bi = 0 (left) and 0.1 (right) with branch (b) under (Pr, Γ, Bd) = (28, 2.0, 0.34) as shown in Fig. 6.

ternational Space Station with a large-scale liquid bridge[21]. It should be noted that Bi must not be zero under the normal gravity as well as microgravity condition even though it would be quite difficult to evaluate Bi. The results by the ground experiments indicate that the flow pattern corresponding to the branch (b) becomes dominant for taller (or high-Γ) liquid bridge[16]. We recognize discripancies between the present LSA and the ground experiments; distributions of Bi over the free surface and ambient temperature, shape of the liquid bridge, temperature dependency of Pr, and so on. We have not reached any concluding ideas to explain the reason why flow patterns corresponding to the branch (b) arise in the ground experiments. And, in the microgravity experiments, the flow pattern corresponding to the branch (b) emerged under Pr = 112, Γ = 3.0 ($AR = H/(2R) = 1.5$ with their definition) and $T_C^* = 15$ °C, but the flow pattern corresponding to the branch (a) or (a') emerged in the same liquid bridge under $T_C^* = 20$ °C[21]. As aforementioned concerning **Fig. 3**, the branch (b) does not appear in a low Bi region under zero gravity condition, and the branches (a) and (a') become most dangerous flow patterns in the range of Bi concerned. It is emphasized, however, that the dynamic Bond number for the liquid bridge in 'Dynamic Surf' would become commensurate to that in the ground experiments by assuming $10^{-3}g_0$ for the residual gravity and 30 mm for the characteristic size of the liquid bridge; that is, zero-Bd experiments were not realized even in low gravity conditions. It is explained that the heat loss to the ambient through the free surface of the liquid bridge would increase if one decreases the cold rod temperature T_C^*. Thus, such variation corresponds to the situation of lower Bi, which agrees qualitatively with the present prediction in spite of large difference in Pr. In addition, microgravity condition would result in less effect of heat loss than that under normal gravity because of less buoyancy effect in the ambient gas motion. Although we have to investigate the Pr effect, we indicate that flow patterns with eigenfunction for the branch (b) would be feasible in the space experiments. Further researches would be needed for comprehensive understandings on the effect of heat transfer against the hydrothermal wave instability especially in large-Pr and/or large-scale liquid bridges.

4. Concluding Remarks

We investigate the effect of heat loss through a free surface on the primary instability of thermocapillary-driven convection in a geometry of so-called half-zone liquid bridge of high Prandtl number fluid by the linear stability analysis. We focus on the flow fields induced by the instability; it is found that the bifurcation diagram exhibits a significant difference between the cases of the Prandtl number Pr = 16 predicted by Xun et al.[24] and 28. The target geometry is the straight liquid bridge whose aspect ratio $\Gamma = H/R$, where H and R are the height and the radius of the bridge, respectively. The effect of gravity level is examined in order to discuss qualitatively the induced flow fields after the transition obtained in the ground-based experiments as well as in on-orbit experiments so-called 'Dynamic Surf' in the Japan Experiment Module 'Kibo' aboard the International Space Station (ISS).

We find that two or three different flow patterns arise in the liquid bridge of Γ = 2.0 depending on the gravity effect. Under the zero gravity condition, the instability brings two flow patterns, named as the branch (a) and (a') in the present study, depending on Bi. In order to distinguish the difference between those two eigenmodes, one has to detect the three dimensional distribution of the flow field or temperature deviation $\hat{T}$. It is indicated that it would be difficult to distinguish the flow patterns (a) and (a') by monitoring the distributions of the temperature over the free surface and the basic flow pattern in $r-z$ plane. We also indicate that a new branch, called (b), emerges in a narrow region near the adiabatic conditions (or small Bi) under small dynamic Bond number condition. A consideration is made why such flow pattern corresponding to the branch (b) was observed in the ground experiments with a small-scale liquid bridge[16], and also in the microgravity experiment known as 'Dynamic Surf' conducted in the Japanese Experiment Module 'Kibo' on the International Space Station[21].

Acknowledgments

We acknowledge Prof. Yasuhiro Kamotani (Case Western Reserve Univ., USA), Prof. Koichi Nishino and Dr. Taishi Yano (Yokohama National Univ., Japan), and Dr. Satoshi Matsumoto (Japan Aerospace Exploration Agency (JAXA)), members of 'Dynamic Surf,' for fruitful discussion.

References

1) M. K. Smith and S. H. Davis: Journal of Fluid Mechanics, **132** (1983) 119.

2) J.-J. Xu and S. H. Davis: Journal of Fluid Mechanics, **161** (1985) 1.
3) Y. Kamotani, L. Wang, S. Hatta, A. Wang and S. Yoda: International Journal of Heat and Mass Transfer, **46** (2003)(17) 3211.
4) F. Preisser, D. Schwabe and A. Scharmann: Journal of Fluid Mechanics, **126** (1983) 545.
5) M. Wanschura, V. M. Shevtsova, H. C. Kuhlmann and H. J. Rath: Physics of Fluids, **7** (1995)(5) 912.
6) J. Leypoldt, H. C. Kuhlmann and H. J. Rath: Journal of Fluid Mechanics, **414** (2000) 285.
7) I. Ueno, S. Tanaka and H. Kawamura: Physics of Fluids, **15** (2003)(2) 408.
8) F. Sato, I. Ueno, H. Kawamura, K. Nishino, S. Matsumoto, M. Ohnishi and M. Sakurai: Microgravity Science and Technology, **25** (2013)(1) 43.
9) T. Matsugase, I. Ueno, K. Nishino, M. Ohnishi, M. Sakurai, S. Matsumoto and H. Kawamura: International Journal of Heat and Mass Transfer, **89** (2015) 903.
10) T. Ogasawara, K. Motegi, T. Hori and I. Ueno: Mechanical Engineering Letters, **5** (2019) $19_0$0014.
11) H. C. Kuhlmann, R. V. Mukin, T. Sano and I. Ueno: Fluid Dynamics Research, **46** (2014) 041421.
12) A. Toyama, M. Gotoda, T. Kaneko and I. Ueno: Microgravity Science and Technology, **29** (2017)(4) 263.
13) M. Irikura, Y. Arakawa, I. Ueno and H. Kawamura: Microgravity Science and Technology, **16** (2005) 176.
14) I. Ueno, A. Kawazoe and H. Enomoto: Fluid Dynamics and Materials Processing (FDMP), **6** (2010)(1) 99.
15) S. Tiwari and K. Nishino: Fluid Dynamics and Materials Processing (FDMP), **6** (2010) 109.
16) I. Ueno, H. Kawasaki, T. Watanabe, K. Motegi and T. Kaneko: Proc. 15th International Heat Transfer Conference (IHTC-15), (2014) ihtc15.
17) D. E. Melnikov and V. M. Shevtsova: Microgravity Science and Technol-ogy, **18** (2006) 128.
18) V. M. Shevtsova, Y. A. Gaponenko and A. A. Nepomnyashchy: Journal of Fluid Mechanics, **714** (2013) 644.
19) D. E. Melnikov and V. M. Shevtsova: International Journal of Heat and Mass Transfer, **74** (2014) 185.
20) V. Yasnou, Y. Gaponenko, A. Mialdun and V. M. Shevtsova: International Journal of Heat and Mass Transfer, **123** (2018) 747.
21) T. Yano, K. Nishino, I. Ueno, S. Matsumoto and Y. Kamotani: Physics of Fluids, **29** (2017) 044105.
22) T. Yano, K. Nishino, S. Matsumoto, I. Ueno, A. Komiya, Y. Kamotani and N. Imaishi: Microgravity Science and Technology, **30** (2018) 599.
23) V. Shevtsova, Y. Gaponenko, H. C. Kuhlmann, M. Lappa, M. Lukasser,
S. Matsumoto, A. Mialdun, J.-M. Montanero, K. Nishino and I. UENO: Fluid Dynamics and Materials Processing, **10** (2014)(2) 197.
24) B. Xun, W.-R. Hu and N. Imaishi: International Journal of Heat and Mass Transfer, **54** (2011) 1698.
25) S. Tiwari and K. Nishino: Journal of Crystal Growth, **300** (2007) 486.
26) H. Kawamura, K. Nishino, S. Matsumoto and I. Ueno: Journal of Heat Transfer, **134** (2012) 031005.
27) T. Yano, K. Nishino, H. Kawamura, I. Ueno and S. Matsumoto: Physics of Fluids, **27** (2015) 024108.
28) K. Nishino, T. Yano, H. Kawamura, S. Matsumoto, I. Ueno and M. K. Ermakov: Journal of Crystal Growth, **420** (2015) 57.
29) J.-J. Xu and S. H. Davis: Physics of Fluids, **27** (1984) 1102.
30) K. Motegi, K. Fujimura and I. Ueno: Physics of Fluids, **29** (2017) 074104.
31) Y. Saad: Numerical methods for large eigenvalue problems: Society for Industrial and Applied Mathematics, 2011, 2nd ed.